RSC Advances

PAPER

View Article Online
View Journal | View Issue

Cite this: *RSC Adv.*, 2023, **13**, 17436

Preparation, performance and mechanism of metal oxide modified catalytic ceramic membranes for wastewater treatment†

Yangbo Huang, *[ab] Zeyu Guan,[a] Qiang Li,[a] Qian Li[c] and Dongsheng Xia[ab]

Catalytic ceramic membranes (CMs) integrated with different metal oxides were designed and fabricated by an impregnation-sintering method. The characterization results indicated that the metal oxides (Co_3O_4, MnO_2, Fe_2O_3 and CuO) were uniformly anchored around the Al_2O_3 particles of the membrane basal materials, which could provide a large number of active sites throughout the membrane for the activation of peroxymonosulfate (PMS). The performance of the CMs/PMS system was evaluated by filtrating a phenol solution under different operating conditions. All the four catalytic CMs showed desirable phenol removal efficiency and the performance was in order of CoCM, MnCM, FeCM and CuCM. Moreover, the low metal ion leaching and high catalytic activity even after the 6th run revealed the good stability and reusability of the catalytic CMs. Quenching experiments and electron paramagnetic resonance (EPR) measurements were conducted to discuss the mechanism of PMS activation in the CMs/PMS system. The reactive oxygen species (ROS) were supposed to be $SO_4^{\bullet-}$ and $^1O_2$ in the CoCM/PMS system, $^1O_2$ and $O_2^{\bullet-}$ in the MnCM/PMS system, $SO_4^{\bullet-}$ and ·OH in the FeCM/PMS system, and $SO_4^{\bullet-}$ in the CuCM/PMS system, respectively. The comparative study on the performance and mechanism of the four CMs provides a better understanding of the integrated PMS-CMs behaviors.

Received 25th February 2023
Accepted 2nd June 2023

DOI: 10.1039/d3ra01291c

rsc.li/rsc-advances

1 Introduction

Membrane-based separation technologies such as the ultrafiltration (UF) process have been widely implemented in industrial wastewater and municipal sewage treatment.[1] UF is usually used as a pretreatment step, with high ability to remove suspended particles, colloids and microorganisms.[2] Ceramic membrane (CM), as a kind of UF made of inorganic materials, has gained lots of momentum during the past decade.[3–5] Compared with organic polymer membranes, ceramic membranes are thermally stable and resistant to chemicals with a lengthy life span, which makes them ideal for organic wastewater purification.[6,7]

However, porous ceramic membranes often exhibit a relatively low rejection rate for many small molecular organics.[8] In addition, membrane fouling is still a critical obstacle that affects membrane performance and limits the wide application of ceramic membranes.[9] To solve these problems, the technology that combines advanced oxidation processes (AOPs) with ceramic membrane separation has recently drawn much attention.[10,11] AOPs are generally conducted with the presence of strong oxidizing species. Common AOPs mainly include photocatalytic oxidation, electro-chemistry oxidation, or activation of superoxides (hydrogen peroxide, ozone and persulfate, *etc.*).[12–14] In the presence of nanocatalysts, peroxides are activated to generate reactive oxygen species (ROS) with high oxidizing potential, which can achieve the catalytic degradation of recalcitrant organic pollutants.[15] The catalysts can be anchored on the surface of membrane or embedded in the pore walls of the internal porous channels. The resultant catalytic membrane has dual functions of filtration and catalytic oxidation, which greatly enhances the removal efficiency of pollutants.[16,17] For one thing, organic contaminants on the membrane surface can be directly oxidized, which significantly alleviates membrane fouling and even achieves *in situ* cleaning of the fouled membrane.[18,19] For another thing, under forced filtration, fluid can bring the reactants to the active catalyst surface, which can enhance mass transfer and achieve a higher catalytic efficiency.[8,20]

Thereby, many researches based on catalytic membrane for wastewater treatment have been reported recently. Wang *et al.* verified that a newly synthesized silicate-based ceramic membrane generated hydroxyl radicals in ozonation process, and this combined process increased the removal rate of *p*-chloronitrobenzene by 50% compared with the ozone-alone process.[21] Park *et al.* developed a catalytic membrane by

[a]*School of Environmental Engineering, Wuhan Textile University, Wuhan, Hubei, 430073, China. E-mail: ybhuang@wtu.edu.cn*

[b]*Engineering Research Center for Clean Production of Textile Dyeing and Printing, Ministry of Education, Wuhan Textile University, Wuhan, Hubei, 430073, China*

[c]*China Three Gorges Corporation, Wuhan, 430014, China*

† Electronic supplementary information (ESI) available. See DOI: https://doi.org/10.1039/d3ra01291c

doping iron oxide nanoparticles on a commercial ceramic membrane and combined the ozonation process for As(III) removal. The catalytic ozonation by the reactive ceramic membrane effectively oxidized As(III) to As(V), which significantly improved the removal rate of As(III) in the hybrid process.[22] Zhu *et al.* sintered a TiO_2 active layer on the Al_2O_3-based ceramic membrane and used the resultant membrane to treat the secondary effluent of the sewage plant. They found that compared with the original membrane, the catalytic membrane showed a higher TOC removal rate and a lower membrane fouling trend.[23] In addition, other excellent studies have also discussed fabrication methods and performance of nanocomposite ceramic membranes for industrial wastewater treatment (such as bisphenol A, dyes, humic acid, *etc.*).[24–28] Researchers generally believe that ceramic membranes with dual functions of catalysis and filtration prepared by modifying the surface of membrane or membrane pore channels have a good application prospect.[10,29]

Among various AOPs, peroxymonosulfate (PMS)-based oxidation technologies have been recently acknowledged as a potential solution for removing toxic and refractory organic pollutants in water.[30] PMS can be easily activated to generate sulfate radical ($SO_4^{\bullet-}$), which is a highly reactive radical with high redox potential (2.5–3.1 V) and long lifetime (30–40 μs).[31] Recent studies have also discovered a non-radical oxidation pathway of PMS, which has high selectivity to specific pollutants and can reduce the production of harmful by-products.[32–34] These enable PMS to effectively react with the target organic pollutants including dyes, perfluorinated compounds, antibiotic and phenol.[35–38] Therefore, PMS advanced oxidation coupled ceramic membrane filtration technology is a promising wastewater treatment method. However, the activation mechanism of PMS by different catalytic membranes and their performance for specific pollutants still need in-deep research.

Until now, some energy-based activation methods (*e.g.*, heat, ultraviolet light, ultrasound and transition metal ions) and heterogeneous activators (metal oxide or carbonaceous materials) were studied to activate PMS.[39] Among them, transition metal oxides have been proved to be efficient, economical and designable catalysts for the degradation of various organic pollutants. However, to the best of our knowledge, few works have reported the systematically comparation of the efficiency and mechanism of transition metal oxides combined ceramic membranes. In this study, a series of metal oxides (Co, Mn, Fe and Cu) modified ceramic membranes were prepared by a facile impregnation-sintering method. Subsequently, the morphology and properties of the resultant catalytic CMs were characterized. Then phenol was selected as the target pollutant to evaluate the performance of different catalytic CMs, and the degradation efficiency of phenol under different membranes and operation conditions was studied. The stability and reusability of the CMs were also investigated. Finally, the main active species for phenol degradation were discussed and the removal pathways were clarified. This work can provide theoretical guidance for the design of efficient metal or bimetal oxide integrated ceramic membranes.

2 Materials and experimental methods

2.1 Materials and reagents

In this work, analytical grade reagents of cobalt nitrate hexahydrate ($Co(NO_3)_2 \cdot 6H_2O$), manganese(II) nitrate tetrahydrate ($Mn(NO_3)_2 \cdot 4H_2O$), copper nitrate trihydrate ($Cu(NO_3)_2 \cdot 3H_2O$), ferrous nitrate ($Fe(NO_3)_3 \cdot 9H_2O$), phenol (C_6H_5OH), sodium hydroxide (NaOH) and sulfuric acid (H_2SO_4) were purchased from Sinopharm Chemical Reagent (China). Methanol (chromatographic grade), *tert*-butyl alcohol (TBA, 98.0%), L-histidine and PMS (available as $2KHSO_5 \cdot KHSO_4 \cdot K_2SO_4$) were bought from Aladdin. Deionized water (18 MΩ cm^{-1}) from a Millipore Milli-Q system was used in all the synthesis and reaction procedures. The initial flat-sheet ceramic membrane (CM) was provided by Huamo Industry Co., Ltd (Shanghai, China), and the detailed features were shown in Table S1.†

2.2 Preparation of metal oxide modified CMs

The catalytic ceramic membranes were prepared by impregnation-sintering method and the preparation process was shown in Fig. S1.† Firstly, the original ceramic membranes were ultrasonically cleaned with deionized water and dried in an oven. Then, the cleaned CMs were divided into four groups and immersed in 0.02 mol L^{-1} $Co(NO_3)_2 \cdot 6H_2O$, $Mn(NO_3)_2 \cdot 4H_2O$, $Cu(NO_3)_2 \cdot 3H_2O$ and $Fe(NO_3)_3 \cdot 9H_2O$ solutions, respectively. The solutions with CMs were sonicated for 10 min to remove any trapped gas bubbles, followed by static immersion for 12 h at 25 °C. Thirdly, the CMs were dried at 60 °C in the oven and then calcinated in the muffle furnace at 240 °C for 4 h. After cooling to room temperature, the CMs was cleaned by deionized water. Four metal oxide modified ceramic membranes were obtained and named as CoCM, MnCM, FeCM and CuCM, respectively.

2.3 Membrane characterizations

The morphology and element content of the synthesized membranes were observed using a Gemini 300 scanning electron microscope (SEM) combined with energy dispersive X-ray spectroscopy (EDS, Oxford X-Max). The components and crystal phase of the materials were characterized by X-ray diffraction (XRD, Bruker D8 Advance) and Fourier transform infrared spectroscope (FTIR, Nicolet, USA). The static contact angle of membrane surface was measured by a DSA 100 instrument (Kruss, Germany), and an average value of five measurements on different membrane locations was recorded. The zeta potential of membrane surfaces was measured using a SurPASS 3 zeta potential analyzer in ultrapure water at pH ranging from 3 to 12. UV-Vis spectrometer were used to measure the concentration of phenol. The ROS generated in CMs/PMS system were identified by electron paramagnetic resonance (EPR). The concentration of leached metal ions from the membrane into the solution was measured by inductively coupled plasma emission spectrometry (ICP, PerkinElmer). Besides, the intermediate products during phenol degradation

were analyzed by a liquid chromatography-mass spectrometry (LC-MS, Thermo Scientific, US).

2.4 Performance evaluation of the combined process of membrane filtration and catalyzed oxidation

Phenol removal efficiency in the combined process of membrane filtration and PMS catalyzed oxidation was evaluated using a bench-scale apparatus as shown in Fig. 1. The ceramic membrane with an effective area of 16 cm^2 was placed in the feed tank with 250 mL of phenol-containing solution. The solution was driven to permeate through the membrane by a peristaltic pump, and the pressure was measured by a pressure gauge. The permeate flux (J_w) of membranes was monitored by an electronic balance and calculated by eqn (1).

$$J = V/(A\Delta t) \quad (1)$$

where V, A and Δt are assigned to the volume of permeate water, the effective area and the operating time.

Before conducting the phenol degradation experiments, the phenol-containing solution was circulated for 30 min to stabilize the system. Subsequently, PMS was added to the solution and start timing. At pre-determined time intervals, 3 mL sample was collected from the feed tank to a PE tube with 100 μL methanol and the concentration of phenol was determined immediately.

In addition, it was reported that a pseudo-first-order equation could be used to describe the kinetics of catalytic degradation.[40] The pseudo-first-order kinetic constant (k_{obs}) is defined as:

$$\ln C/C_0 = -k_{obs} \cdot t \quad (2)$$

where C, C_0 and t are assigned to the concentration of phenol, the initial phenol concentration and reaction time, respectively.

The initial pH of the solution was adjusted using 0.05 M NaOH and H_2SO_4. When evaluating the reusability of the CMs, the membrane was rinsed with 500 mL water after each experiment and dried at 60 °C before next use.

3 Results and discussion

3.1 Characterization of catalytic CMs

SEM and EDS mapping were used to observe the surface morphology and elemental distribution of the metal oxide modified ceramic membranes, and the results were shown in Fig. 2. Both pristine and modified membranes exhibited rough and porous surfaces. Compared with the virgin CM, except for the appearance of some nanoparticle agglomeration phenomena, the morphology of the modified CMs did not change dramatically. These may be due to the small amount of metal oxide particles coated onto membrane surfaces (Table S2†). The images of EDS mapping also exhibited that the elemental abundance of Co, Mn, Fe and Cu is significantly less than that of Al on the substrates. In addition, EDS results further proved that the metal oxide particles fully covered and uniformly dispersed on membrane surfaces.

The hydrophilicity of membrane surfaces was characterized by static contact angle and the results were shown in Fig. 3a. The contact angle on the surface of all the four metal oxide modified CMs decreased from 40° to around 22°. In comparison, the modified membranes all exhibited better wettability than the pristine CM, owing to the hydroxyl groups covered on the surface of metal oxide particles.[41]

The zeta potential of membrane surface was measured at pH ranging from 3 to 12. As shown in Fig. 3b, they gradually decreased with increasing the pH value, which were consistent

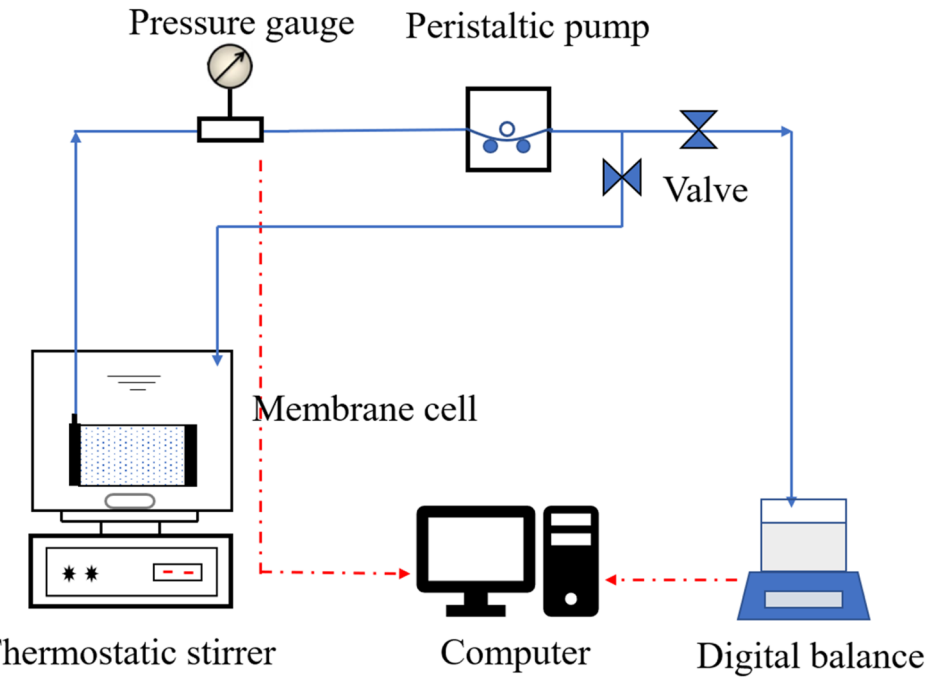

Fig. 1 Schematic diagram of the membrane filtration system.

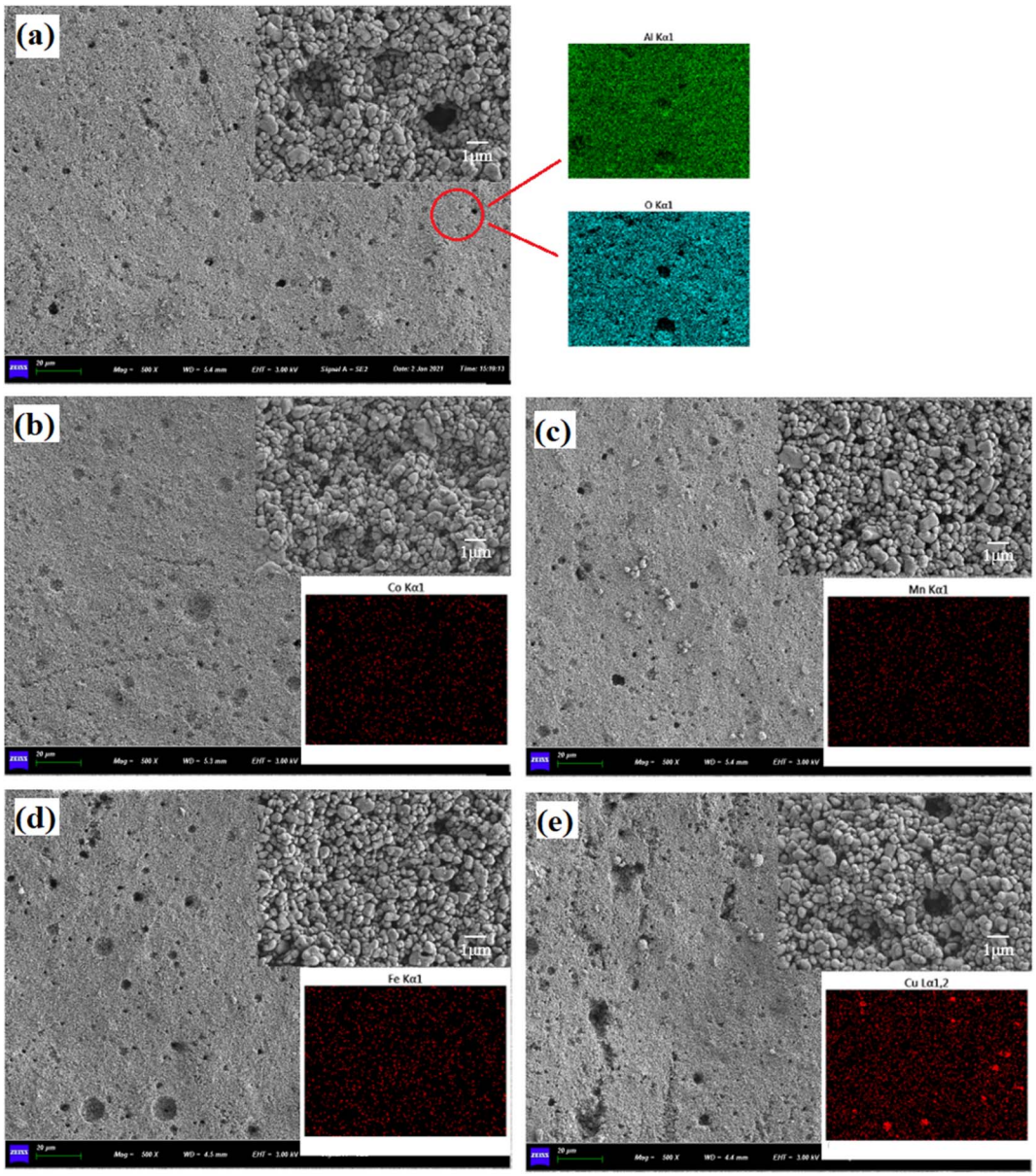

Fig. 2 The surface morphology and EDS mapping of the CMs. (a) The pristine CM, (b) CoCM, (c) MnCM, (d) FeCM and (e) CuCM.

with the similar trend of metal oxide nanoparticles reported elsewhere.[42,43] Compared with the pristine CM, the zeta potentials of all the modified CMs changed more obviously with pH. This could be also attributed to the hydroxyl groups (Me–OH) covered on the surface of metal oxide particles, which experienced a protonation–deprotonation process under different pH conditions. The point of zero charge (pH_{pzc}) of pristine CM is about 6.5, while that of the modified CMs were ranging from 5.3 to 9.3.

In order to analyze the component and crystalline structure of the modified CMs, the FTIR spectrums and XRD tests were measured and CoCM was taken as an example in Fig. 4. As shown in Fig. 4a, the absorption peaks at 3300 cm^{-1} and 1630 cm^{-1} corresponded to O–H stretching and bending vibrations, which also suggested the presence of hydroxyl groups on membrane surfaces.[43] And the stronger peak intensity on CoCM membrane indicated that more hydroxyl groups covered on the modified membrane surface. This was consistent with the results of the contact angle measurements. Fig. 4b showed the XRD patterns for surface component of pristine CM and CoCM. The characteristic peaks at 25.6, 35.1, 37.8, 43.4, 52.6, 57.5, 66.5, 68.2, and 76.9° could be ascribed to (012), (104), (110), (113), (024), (116), (214), (300) and (119) crystal planes of Al_2O_3 (PDF#78-2426). This was because the main component of the CMs was Al_2O_3. However, no significant signals of Co were observed in both FTIR and XRD spectrums. This may be due to the low content and high dispersion of catalysts loadings. Therefore, to clarify the specific composition of the metal oxides on the membrane, catalyst particles were synthesized under the same conditions as the preparation of CMs. Fig. S2† showed the

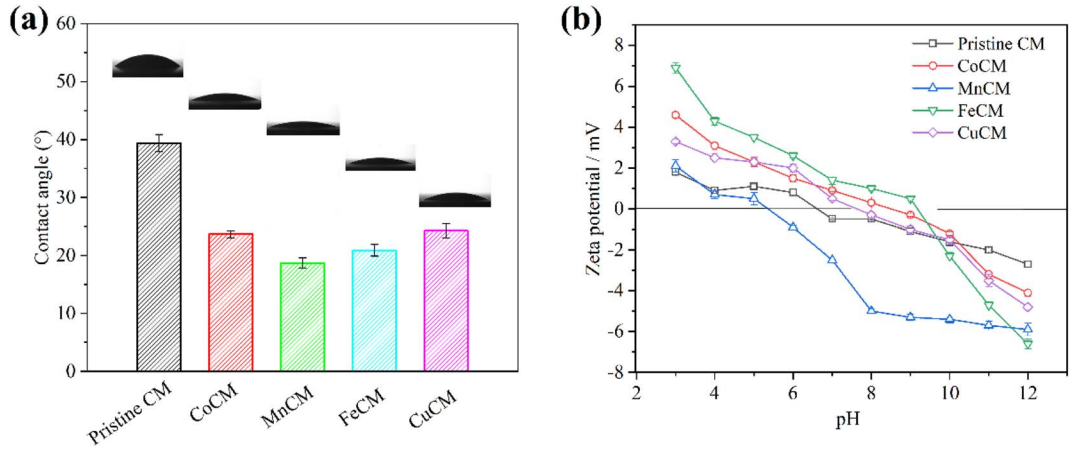

Fig. 3 The contact angles (a) and zeta potentials (b) of the CMs.

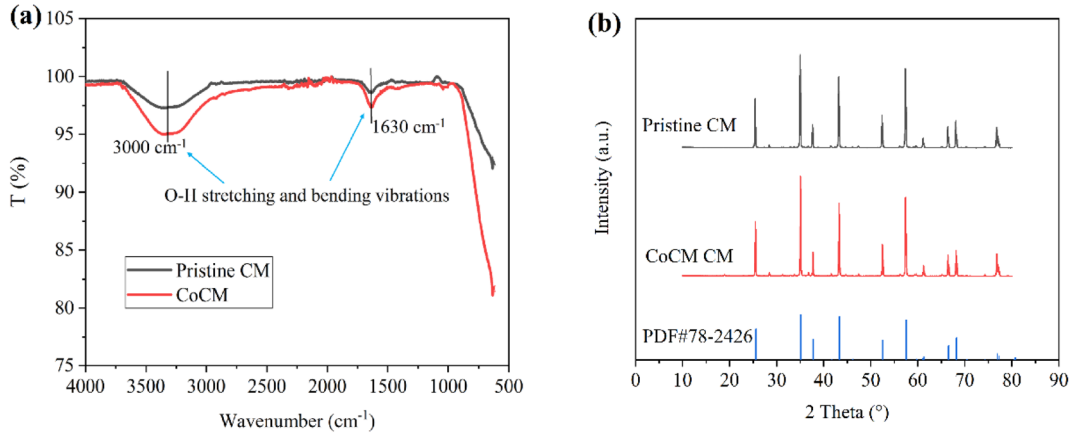

Fig. 4 The FTIR spectra (a) and XRD analysis (b) of the pristine CM and CoCM.

XRD patterns of the four metal oxides. It could be seen that the catalysts coating on the four CMs were Co_3O_4 (PDF#74-2120), MnO_2 (PDF#81-2261), Fe_2O_3 (PDF#79-1741) and CuO (PDF#48-1548), respectively. In addition, it should be noted that the catalysts on MnCM may also contain small amounts of Mn_3O_4 (PDF#76-0150) due to the characteristic peak at 33.0°.

The cross section of the CMs were also characterized by SEM-EDS and the results were depicted in Fig. 5. The SEM images clearly showed that the prepared CMs consist of two layers: a dense layer and a support layer. The thickness of the dense layer was about 15 μm. Compared to the pristine CM, the cross-section morphologies of modified CMs changed significantly. It appeared that some catalysts were coated onto the inner structure of the membranes, which was also confirmed by the EDS mapping. The EDS mapping images showed that all the four catalysts were successfully and uniformly integrated to the porous channels of the membranes, which was critical for the catalytic degradation of organics as the activation of PMS could be facilitated within the pores of the catalytic membrane. Table S3† showed the cross-section element compositions of the CMs. The catalyst content inside the membrane was much higher than the surface (Table S2†), which was mainly due to the larger surface area of the porous structure inside the membrane. Therefore, the well-distributed metal oxide particles would play an important role in the CM/PMS system to degrade refractory organics.

Furthermore, although the catalysts were loaded into the membrane pores, the water permeation performance of the membrane was not negatively affected. As shown in Fig. 6, the performance of different CMs in filtration of phenol solution was evaluated. The results showed a slight increase in water flux of the modified CMs, which may be attributed to the improvement of hydrophilicity. However, all the CMs showed a very low phenol retention rate (below 7%) and the retention rate could be mainly attributed to the adsorption of phenol by the membrane. The results also illustrated the necessity of combining the microporous ceramic membrane with the advanced oxidation process to enhance the removal of organic matters.

3.2 Performance evaluation of catalytic CMs

3.2.1 Efficiency of phenol degradation. Before investigating the catalytic degradation of phenol during PMS-based catalytic CMs filtration process, it was important to access whether the

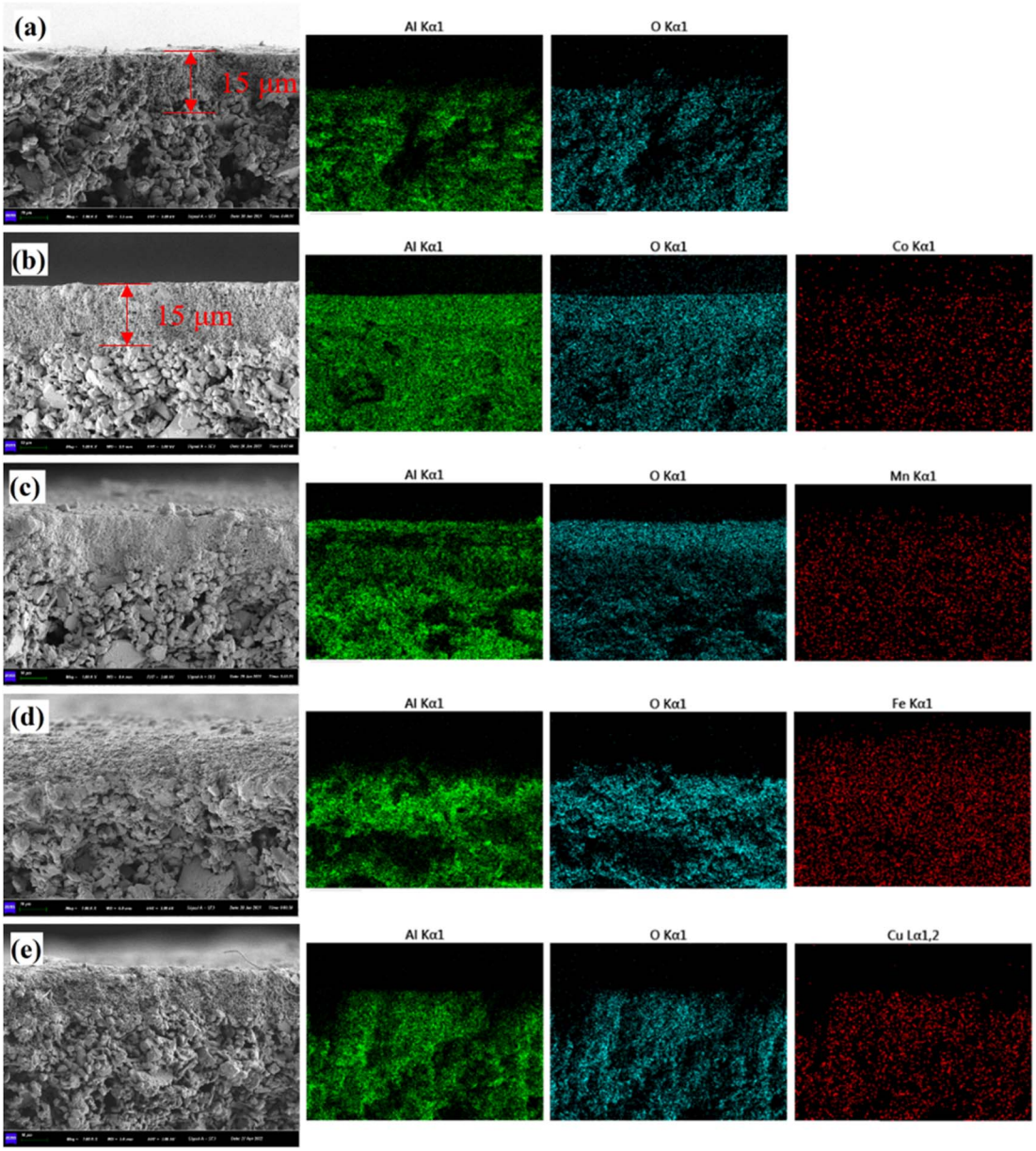

Fig. 5 The SEM images and EDS mapping of the CMs. (a) the pristine CM, (b) CoCM, (c) MnCM, (d) FeCM and (e) CuCM.

contaminants could be removed by pristine CM or PMS alone, or a combination of both. Accordingly, comparative experiments were carried out on the above problems and the results were depicted in Fig. S3.† The results showed that the adsorption of phenol by the pristine CM was negligible and could be excluded as a possible mechanism. The direct oxidation efficiency of phenol by PMS was about 8%, and the oxidation products were mainly benzoquinone (Fig. S4†). Furthermore, results also showed that the pristine CM could not activate PMS to enhance phenol removal. Therefore, it is necessary to load metal oxide catalysts on ceramic membranes.

Fig. S5† compared the phenol and TOC removal rate of the four membrane systems. Comprehensively, it could be concluded that under the same operation conditions, the degradation efficiency of phenol in different CMs/PMS systems was in order of CoCM > MnCM > FeCM > CuCM. The phenol removal rate was 100%, 99%, 87%, 83% for CoCM, MnCM, FeCM and CuCM, while the corresponding TOC removal rate was 88%, 82%, 74% and 70%, respectively. The difference in membrane catalytic performance may be mainly attributable to the types and production mechanism of ROS, which will be analyzed in detail in the activation mechanism section. Besides, comparison of the literature with this work on degradation efficiency of phenol by catalytic membranes is summarized in Table S4.† It can be seen that the four CMs in this work have advantages in phenol wastewater treatment.

3.2.2 Effect of solution pH. As we know that the performance of PMS-based AOPs is greatly affected by the solution pH. Accordingly, the catalytic degradation of phenol in modified-CMs/PMS system was investigated at pH value of 3, 7 and 11.

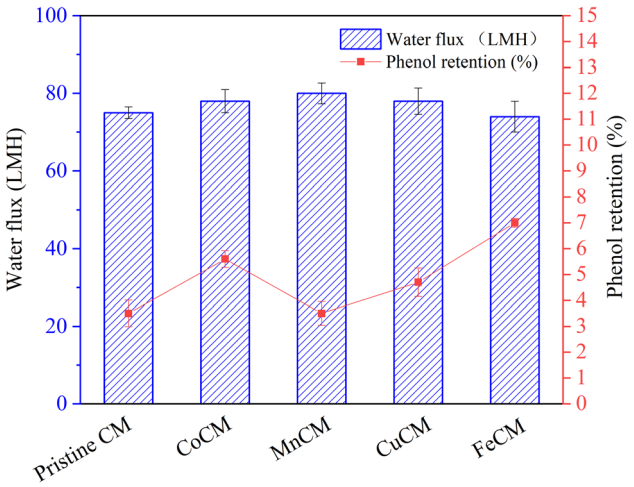

Fig. 6 The water flux and phenol retention of the CMs in filtration of phenol solution (30 mg L^{-1}, 60 kPa).

As shown in Fig. 7, the optimum solution condition of all the four modified CMs was acidic. This may be related to the zeta potential of the membranes. The surface charge of the CMs had an influence on the adsorption of pollutants and oxidants.[44] As shown in Fig. 4, the pH_{pzc} of CMs were ranging from 5.3 to 9.3. In acidic solution, the membranes were positively charged and the phenol was mainly in the form of C_6H_5OH ($pK_a = 9.96$) while the primary PMS species were HSO_5^-. Therefore, the acidic condition would favor the interaction between CMs and HSO_5^- to effectively generate reactive oxygen species.

CoCM was used as an example to discuss the change of reaction rate with pH value. The results presented in Fig. 7a demonstrated that as the pH decreased from 11 to 3, the reaction rate constant k_{obs} increased from 0.074 to 0.196 min^{-1} and phenol was completely oxidized under acid conditions within 30 min. However, under alkaline conditions, approximately 12% of the phenol was still not be removed after 60 min. In general, the CoCM/PMS system showed good applicability at pH value from 3 to 11.

3.2.3 Effect of PMS concentration. Fig. 8 illustrated the catalytic degradation of phenol by CMs at different PMS concentrations. A dramatic increase of degradation efficiency was achieved for all the for CMs with the PMS concentration increased from 1 mM to 2 mM. Take CoCM as an example, when the PMS concentration was 1 mM, less than 80% of phenol was degraded after reaction for 30 min, whereas more than 96% of phenol was removed within 30 min at a PMS concentration of 2 mM. Higher PMS concentration increased the probability of CMs interacting with oxidant molecules, promoting the

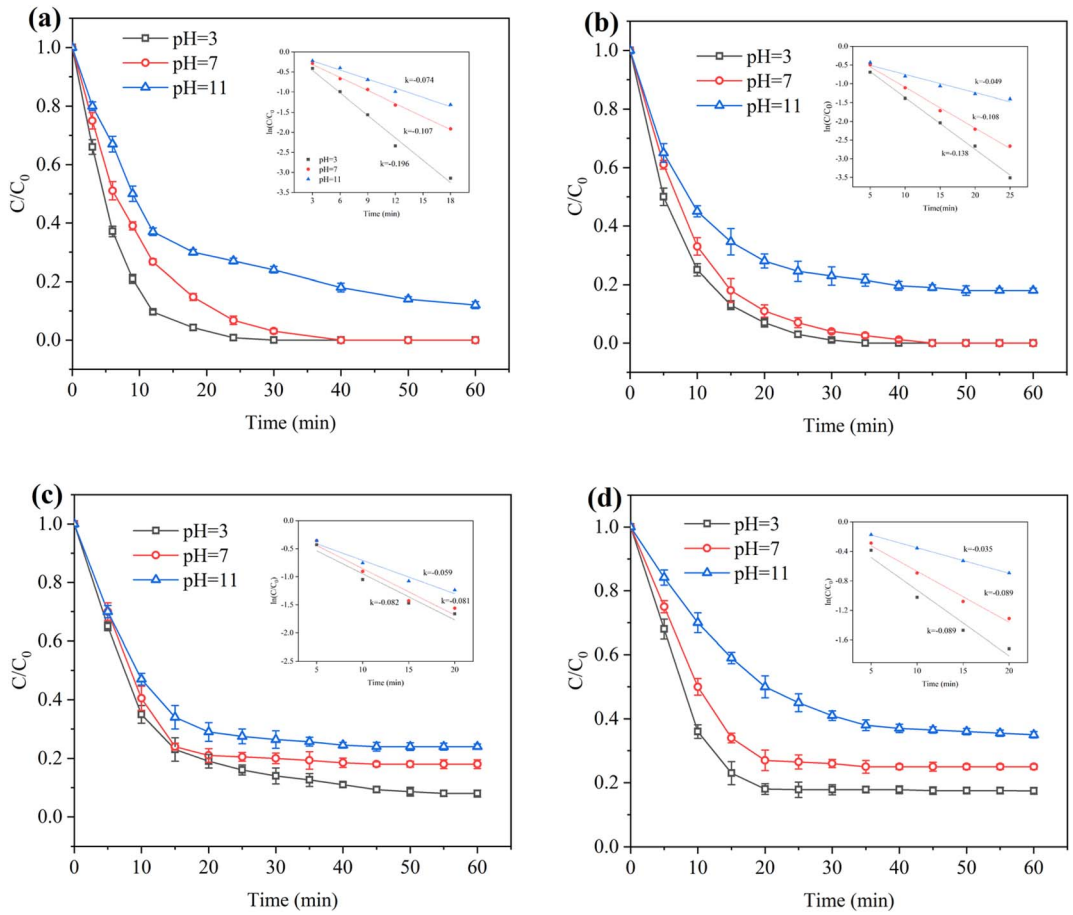

Fig. 7 Effect of initial pH on the degradation of phenol. (a) CoCM, (b) MnCM, (c) FeCM, (d) CuCM. Experimental conditions: $C_{phenol} = 30$ mg L^{-1}, $C_{PMS} = 2$ mM, $T = 25$ °C.

activation of PMS to rapidly generate reactive oxygen species, possibly resulting in increased phenol decomposition.[8] The k_{obs} values of CoCM were 0.051, 0.111, 0.132 min^{-1} at a PMS concentration of 1, 2, 5 mM, respectively, indicating that the improvement in phenol degradation performance was limited when the PMS dosage continued to increase from 2 to 5 mM. This may be due to the limited number of catalysts on the membrane interface, which constrained the rate of PMS activation.[45] So, no obvious rise of ROS concentration in the solution with the excess PMS. Moreover, it was reported that the excess HSO_5^- would consume $SO_4^{\bullet-}$ and led to a reduction in the total amount of free radicals in solution.[46,47] Considering the similar removal rate of 2 mM and 5 mM, the former was chosen as the optimum amount of PMS.

3.2.4 Effect of phenol concentration. The degradation efficiency of phenol by CMs with respect to different initial concentration was investigated and the results were shown in Fig. 9. A dramatic decline of degradation efficiency was observed with the initial concentration increased from 10 to 50 mg L^{-1}. The calculated k_{obs} of phenol degradation by CoCM was 0.226, 0.111 and 0.063 min^{-1} when the initial phenol concentration was 10, 20 and 50 mg L^{-1}, respectively.

It was reported that the relationship between $\ln(k_{obs})$ and logarithms of experimental parameters could reflect which factor was more sensible to phenol removal efficiency by CMs/PMS system.[48,49] Fig. S6† showed that the $\ln C_{PMS}$ and $\ln C_{phenol}$ had good linearity with $\ln(k_{obs})$, and the corresponding slopes were 0.909 and 0.767, respectively. Larger slope means it was a more important factor determining the degradation rate for CMs/PMS system. These results indicated that the influences of the two parameters were in the order of $C_{PMS} > C_{phenol}$. Thus, in practical applications, when the CMs/PMS system is used to treat high-concentration phenol wastewater, the dosage of PMS should also be increased accordingly.

3.3 Stability and reusability of catalytic CMs

In order to maintain high catalytic activity for long time operation, the modified CMs should have a stable structure and good reusability. The stability of CMs was accessed by measuring the concentration of leached metal ions from the membrane into the solution. Fig. 10a showed that all metal ions in the membrane composition were detected after the first cycle (30 min per cycle). The concentration of Co, Mn, Fe and Cu leached from different CMs were 7.1, 3.6, 4.6, 3.1 μg L^{-1}, respectively, which were all at a relatively low level. Referring to the Chinese surface water quality standards (GB3838-2002: [Co] ≤ 1.0 mg L^{-1}, [Fe] ≤ 0.3 mg L^{-1}, [Mn] ≤ 0.1 mg L^{-1}, [Cu] ≤

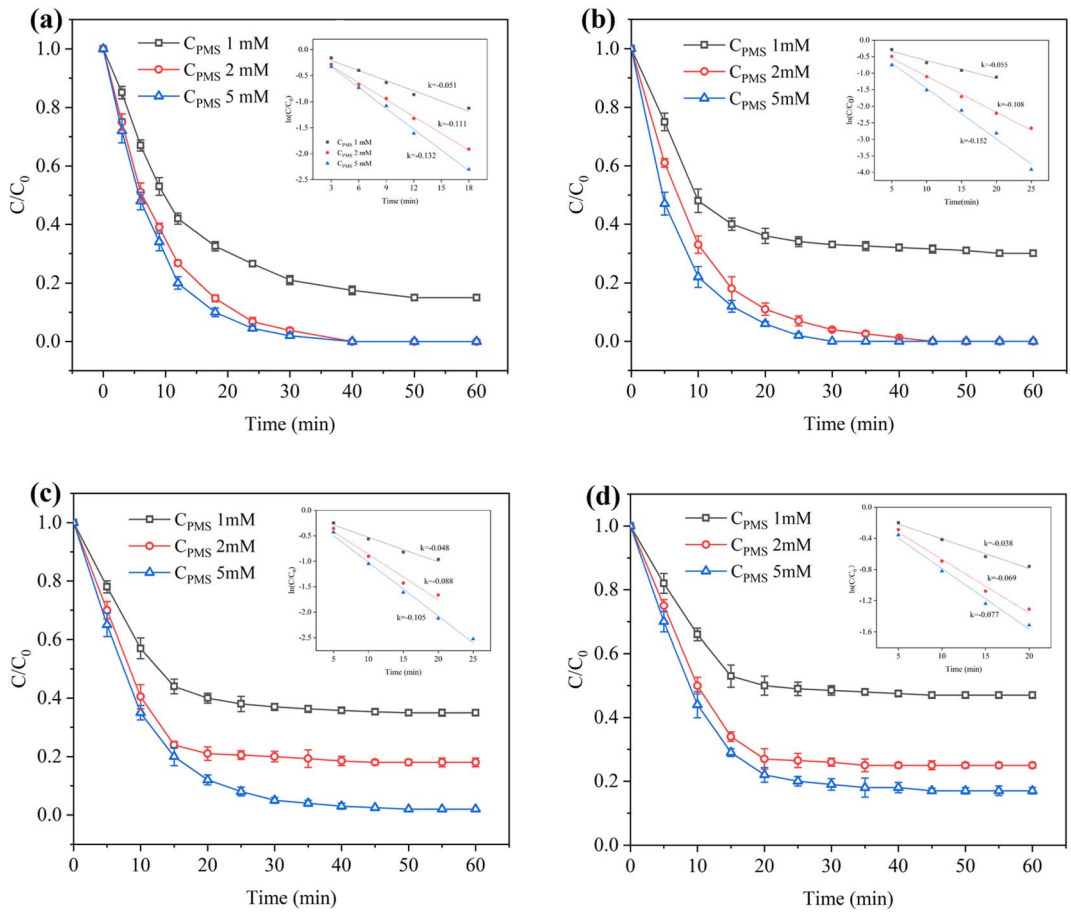

Fig. 8 Effect of PMS concentration on the degradation of phenol. (a) CoCM, (b) MnCM, (c) FeCM, (d) CuCM. Experimental conditions: C_{phenol} = 30 mg L^{-1}, pH = 7, T = 25 °C.

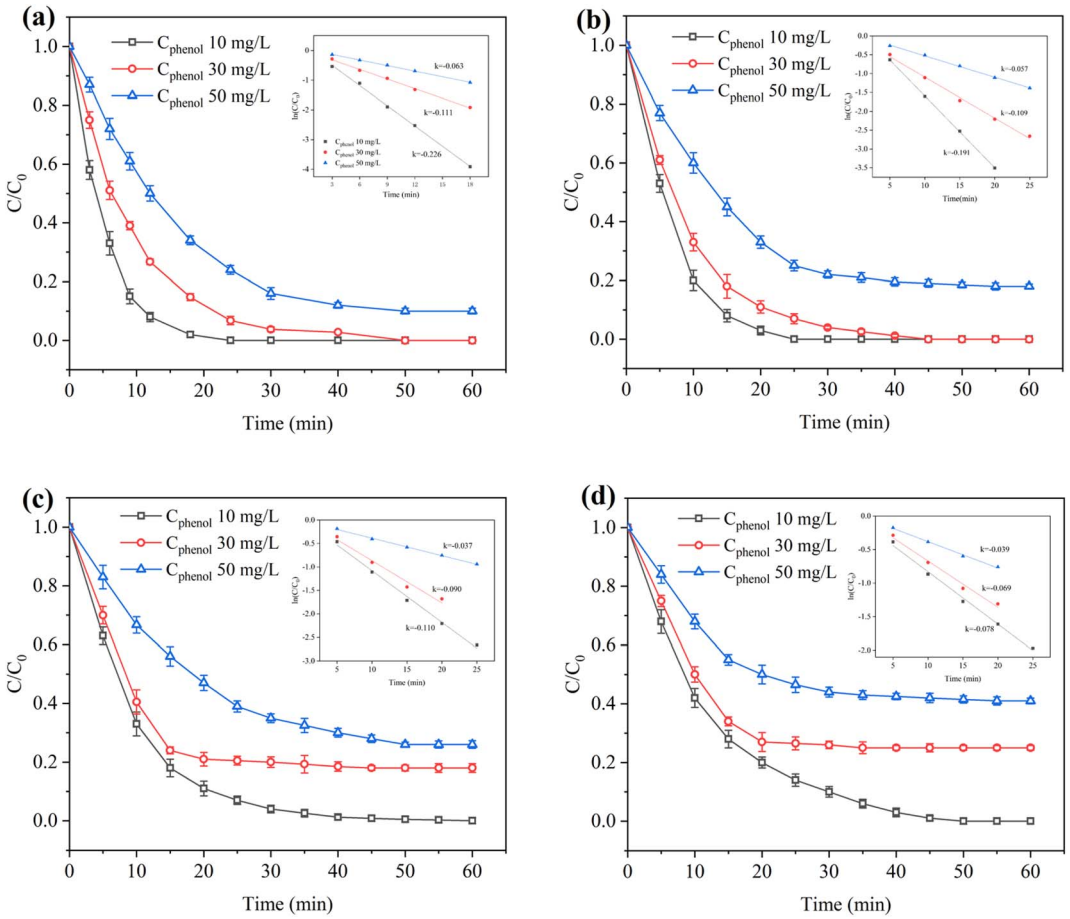

Fig. 9 Effect of phenol concentration on the degradation efficiency. (a) CoCM, (b) MnCM, (c) FeCM, (d) CuCM. Experimental conditions: C_{PMS} = 2 mM, pH = 7, T = 25 °C.

1.0 mg L^{-1}), the concentration of these leached heavy metal ions was within the safe range.[50] In addition, aluminum ions, which were the main body of all CMs, were also detected at a concentration of about 30 μg L^{-1}. Trace amounts of Al leaching could be considered a normal phenomenon under acidic conditions (pH = 3).[27]

Additionally, take CoCM as an example, the effect of metal ions leaching on the performance of the modified CMs was studied. As shown in Fig. 10b, the CoCM could still maintain a high catalytic activity after multiple runs. The phenol removal efficiency declined about 5.5% throughout six cycles. This may be due to the shielded active sites by contaminants during degradation.[8] Besides, the variation of metal leakage during several cycles of uses was also studied. It can be seen from Fig. 10c that the maximum amount of metal leakage was occurred at the first cycle, then gradually decreased. In all, the properties of low metal ion leaching, high catalytic activity and good reusability indicate that the catalytic CMs has a promising prospect in degradation of organic pollutants.

3.4 Reactive species in CMs/PMS system

Radical and non-radical oxidation pathways may exist in the PMS-based AOPs during the degradation of organic contaminants. Quenching experiments were conducted to identify the ROS for phenol removal in CMs/PMS system. Methanol (MeOH) was used as the scavenger of both ·OH and $SO_4^{\cdot-}$ with apparent rate constants of (1.6–7.7) × 10^7 M^{-1} s^{-1} and (1.2–2.8) × 10^9 M^{-1} s^{-1}, respectively. *Tert*-Butyl alcohol (TBA) was used for quenching ·OH as it reacts much faster with ·OH ((3.8–7.6) × 10^8 M^{-1} s^{-1}) than $SO_4^{\cdot-}$ ((4.0–9.1) × 10^5 M^{-1} s^{-1}). Fig. 11a illustrated the quenching tests after addition of MeOH and TBA, and CoCM was used as an example to discuss (the results of MnCM, FeCM and CuCM were depict in Fig. S6†). The removal rate of phenol reduced by 45.0% with the introduction of MeOH, while the effect of TBA was not significant. This indicated that $SO_4^{\cdot-}$ contributed greatly to phenol degradation than ·OH and the effect of ·OH was negligible. In addition, superoxide radicals ($O_2^{\cdot-}$) were identified by p-BQ. As depicted in Fig. 11a, the removal efficiency decreased only 20.4% in the presence of 10 mM p-BQ, implying that the direct degradation of phenol by $O_2^{\cdot-}$ is limited. It was reported that $O_2^{\cdot-}$ was usually generated by the decomposition of the PMS and would further convert to $^1O_2$.[51,52] Therefore, non-radical oxidation pathway ($^1O_2$) in this study was investigated by adding L-histidine into the CMs/PMS system. As shown in Fig. 11b, the removal of phenol gradually decreased to 17.3% with the

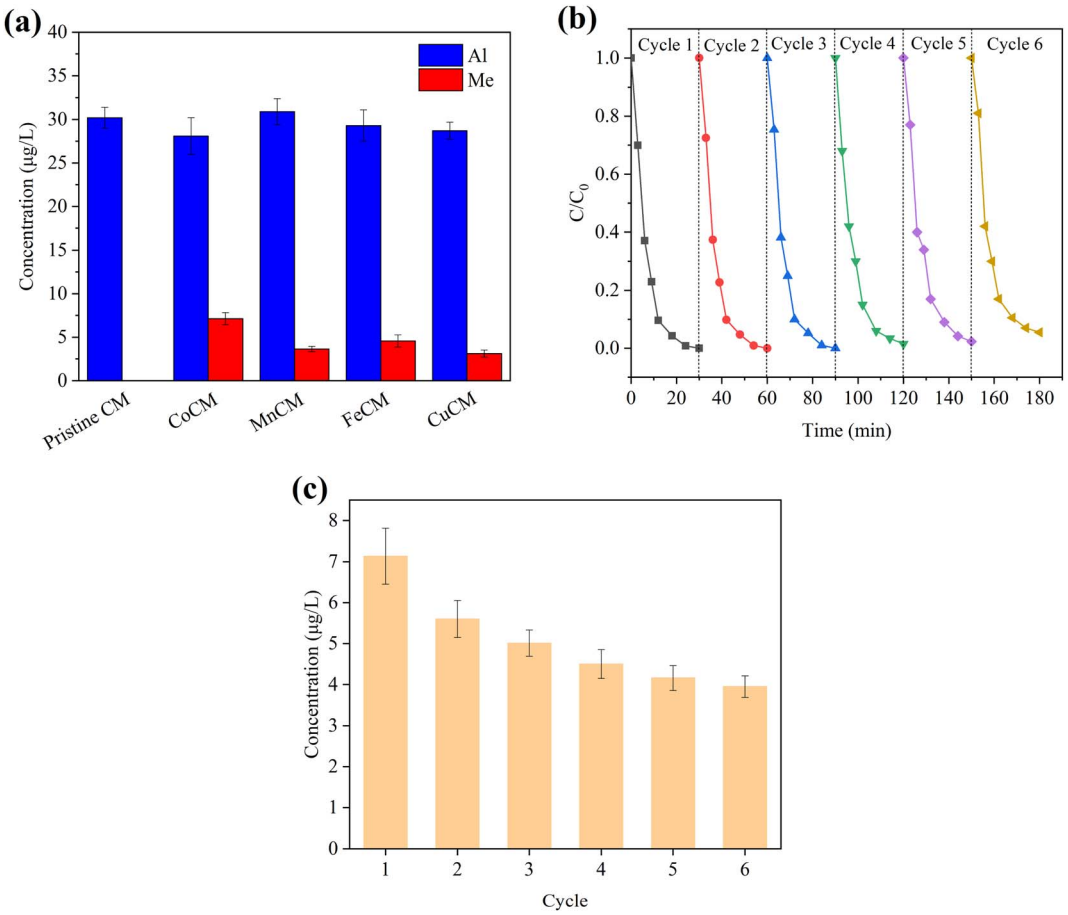

Fig. 10 (a) The concentration of leached metal ions from the membrane into the solution in the first cycle, (b) reuse of CMs in the degradation process and (c) Co leakage during several cycles of uses. Experimental conditions: C_{phenol} = 30 mg L^{-1}, C_{PMS} = 2 mM, pH = 7, T = 25 °C.

adding of 20 mM L-histidine, suggesting that $^1O_2$ was generated and played a dominant role in the degradation of phenol by CMs/PMS system.

Furthermore, EPR technology was used to verify the ROS in the CMs/PMS systems by introducing DMPO and TEMP as spin-trapping agent. As shown in Fig. 11c and d, three characteristic peaks were observed in the CoCM/PMS system, which corresponded to DMPO–$SO_4^{\cdot-}$, DMPO–·OH and TEMP-$^1O_2$, respectively. Additionally, due to the short half-life of $O_2^{\cdot-}$, MeOH was used instead of water as the solvent to capture $O_2^{\cdot-}$ by DMPO. The resultant quadruple peak in Fig. 11c corresponded to DMPO–$O_2^{\cdot-}$, indicating the existence of $O_2^{\cdot-}$ in the CoCM/PMS system.

Based on the results and detail analysis above, the possible mechanism for PMS activation by CoCM was proposed in eqn (3)–(7). Co(III) preliminarily reacted with PMS to produce $SO_5^{\cdot-}$ and Co(II), and then the converted Co(II) could further activate PMS to generate $SO_4^{\cdot-}$ and ·OH with the regeneration of Co(III).

$$\equiv Co(III) + HSO_5^- \rightarrow \equiv Co(II) + SO_5^{\cdot-} + H^+ \quad (3)$$

$$\equiv Co(II) + HSO_5^- \rightarrow \equiv Co(III) + SO_4^{\cdot-} + OH^- \quad (4)$$

$$SO_4^{\cdot-} + OH^- \rightarrow {}^{\cdot}OH + SO_4^{2-} \quad (5)$$

$$3HSO_5^- + H_2O \rightarrow 3SO_4^{2-} + 2O_2^{\cdot-} + 5H^+ \quad (6)$$

$$2O_2^{\cdot-} + 2H_2O \rightarrow {}^1O_2 + H_2O_2 + 2OH^- \quad (7)$$

Thus, the two experiments of quenching and EPR jointly corroborated that the reactive oxygen species of $SO_4^{\cdot-}$, ·OH, $O_2^{\cdot-}$and $^1O_2$ were generated during degradation of phenol by CMs. Among them, $^1O_2$ and $SO_4^{\cdot-}$ were considered to be the main active species for phenol degradation in the CoCM/PMS system with the order of $^1O_2$ > $SO_4^{\cdot-}$. These results were similar to Li's report on the mechanism of PMS activation.[45]

Besides, it could be concluded from Fig. S7† that the dominating ROS for phenol degradation in the other three membrane system were quite different from the CoCM/PMS system. The dominating ROS were speculated to be $^1O_2$ and $O_2^{\cdot-}$ in the MnCM/PMS system, $SO_4^{\cdot-}$ and ·OH in the FeCM/PMS system, $SO_4^{\cdot-}$ in the CuCM/PMS system, respectively. Thus, the oxidation mechanism is quite complex in different CM/PMS systems. For example, some researcher also reported that the activated PMS on CuO surface through direct electron transfer contribute a lot in the CuO/CMs system.[53,54] The possible catalytic mechanism for PMS activation by other CMs were listed in ESI Text S1.†

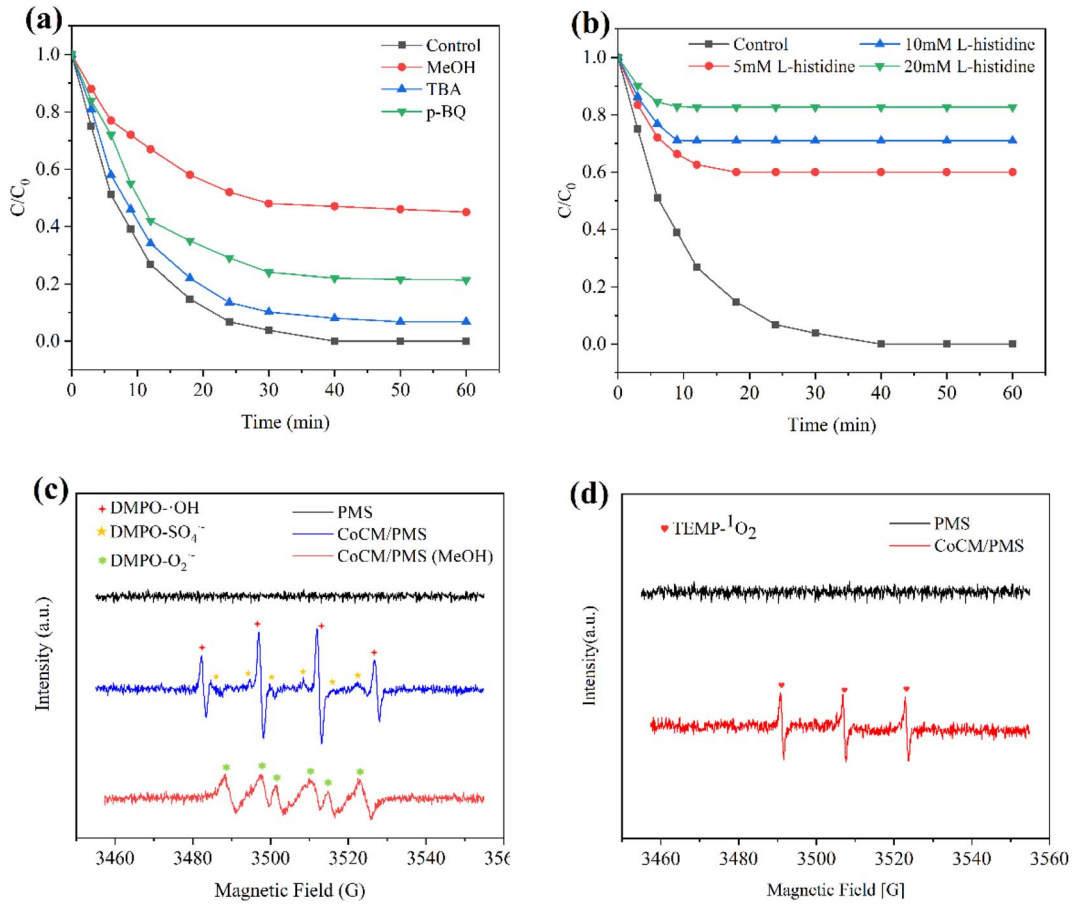

Fig. 11 (a and b) Quenching experiments and (c and d) EPR spectra. Experimental conditions: $C_{PMS} = 2$ mM, $C_{phenol} = 30$ mg L^{-1}, pH = 7.0, $C_{MeOH} = 500$ mM, $C_{TBA} = 500$ mM, $C_{p\text{-}BQ} = 10$ mM, $C_{DMPO} = 100$ mM, $C_{TEMP} = 100$ mM.

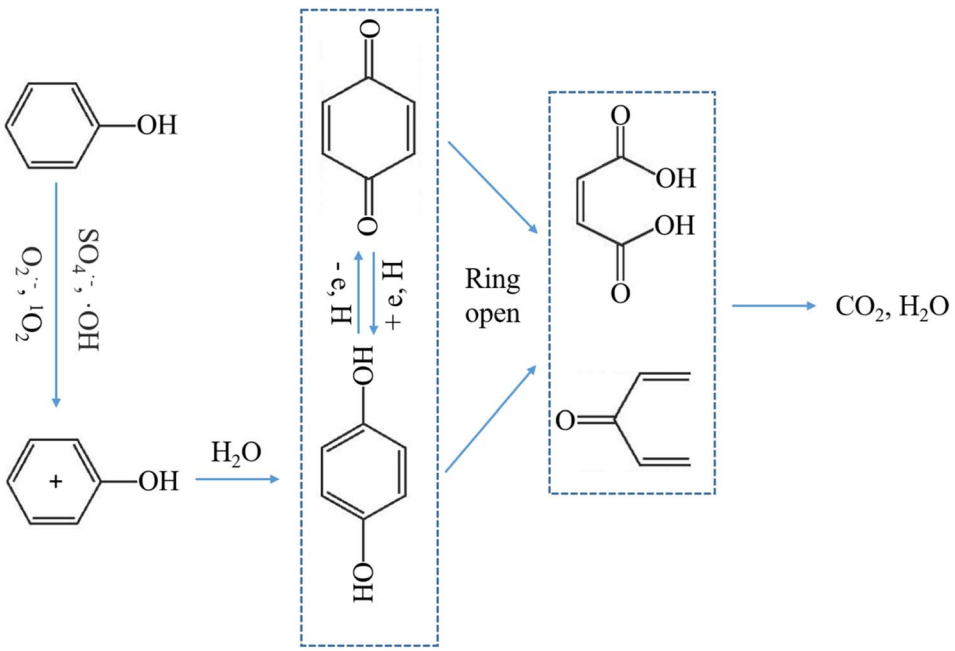

Fig. 12 Proposed degradation pathways of phenol in CoCM/PMS system. Experimental conditions: $C_{PMS} = 2$ mM, $C_{PMS} = 30$ mg L^{-1}, pH = 7.0.

3.5 Investigation of phenol degradation pathway

Intermediate products during phenol degradation process in the CoCM/PMS system were detected by LC-MS. As shown in Fig. S8,† three oxidation intermediates were identified, including hydroquinone ($m/z = 110$), *p*-benzoquinone ($m/z = 108$) and penta-1,4-dien-3-one ($m/z = 81$). Based on the results of LC-MS, the degradation pathway of phenol was speculated and illustrated in Fig. 12. Firstly, benzene ring was attacked by $SO_4^{\cdot-}$ and $^1O_2$ to form a cation radical, which subsequently converted to hydroquinone.[45] Hydroquinone is not a very stable substance that can be easily oxidized to *p*-benzoquinone. Next, *p*-benzoquinone and hydroquinone were further oxidized by $SO_4^{\cdot-}$ and $^1O_2$ and the ring-opening reaction occurred, producing 1,4-dien-3-one and fumaric acid. Then all the small molecules of ring-opening products could be eventually mineralized into CO_2 and H_2O.

4 Conclusion

In summary, four kinds of metal oxides modified ceramic membranes (CMs) were fabricated by impregnation-sintering method and used for the catalytic degradation of phenol. The catalyst particles (Co_3O_4, MnO_2, Fe_2O_3 and CuO) were fully anchored and uniformly dispersed on membrane surfaces and the internal porous channels, which was critical for the catalytic degradation of organics as the activation of PMS could be facilitated within the pores of the catalytic membrane. Compared to the pristine CM, the modification improved membrane hydrophilicity, water permeability and phenol retention rate. Under the same operation conditions, the degradation efficiency of phenol in different CMs/PMS systems was as follows: CoCM > MnCM > FeCM > CuCM. In addition, quenching tests and EPR measurements demonstrated that the dominating ROS were speculated to be $SO_4^{\cdot-}$ and $^1O_2$ in the CoCM/PMS system, $^1O_2$ and $O_2^{\cdot-}$ in the MnCM/PMS system, $SO_4^{\cdot-}$ and ·OH in the FeCM/PMS system, $SO_4^{\cdot-}$ in the CuCM/PMS system, respectively. Finally, the properties of low metal ion leaching, high catalytic activity and good reusability indicate that the catalytic CMs has a promising prospect in degradation of organic pollutants.

Conflicts of interest

The authors declare that they have no known competing financial interests or personal relationships that could have appeared to influence the work reported in this paper.

Acknowledgements

This work was financially supported from the Central government guidance for local science and technology development projects for Hubei province (No. 2020ZYYD038).

References

1 Y. Ren, Y. Ma, G. Min, W. Zhang, L. Lv and W. Zhang, *Sci. Total Environ.*, 2020, **762**, 143083.
2 N. K. Khanzada, M. U. Farid, J. A. Kharraz, J. Choi, C. Y. Tang, L. D. Nghiem, A. M. Jang and A. K. An, *J. Membr. Sci.*, 2020, **598**, 117672.
3 R. Miao, B. Ma, P. Li, P. Wang and X. Y. Li, *J. Membr. Sci.*, 2021, **629**, 119307.
4 D. Wei, T. Yi, Z. Zhang, L. Liu and X. Zhang, *J. Membr. Sci.*, 2016, **498**, 116–124.
5 E. Alventosa-Delara, S. Barredo-Damas, M. I. Alcaina-Miranda and M. I. Iborra-Clar, *J. Hazard. Mater.*, 2012, **209**, 492–500.
6 S. M. Samaei, S. Gato-Trinidad and A. Altaee, *Sep. Purif. Technol.*, 2018, **200**, 198–220.
7 M. B. Asif and Z. Zhang, *Chem. Eng. J.*, 2021, **418**, 129481.
8 Y. Fan, Y. Zhou, Y. Feng, P. Wang, X. Li and K. Shih, *J. Membr. Sci.*, 2020, **611**, 118302.
9 Z. Bai, R. Zhang, S. Wang, S. Gao and J. Tian, *Sep. Purif. Technol.*, 2021, **274**, 118951.
10 K. Plakas, A. Mantza, S. Sklari, V. Zaspalis and A. Karabelas, *Chem. Eng. J.*, 2019, **373**, 700–708.
11 W. Jiang, X. Xia, J. Han, Y. Ding, R. H. Muhammad and A. Wang, *Environ. Sci. Technol.*, 2018, **52**, 9972–9982.
12 H. Wu, X. Xu, L. Shi, Y. Yin, L. Zhang, Z. Wu, X. Duan, S. Wang and H. Sun, *Water Res.*, 2019, **167**, 115110.
13 X. Duan, H. Sun, Z. Shao and S. Wang, *Appl. Catal., B*, 2018, **224**, 973–982.
14 X. Duan, H. Sun, M. Tade and S. Wang, *Catal. Today*, 2018, **307**, 140–146.
15 D. He, Y. Li, L. Cong, L. Song and S. Zhang, *Chemosphere*, 2020, **255**, 126961.
16 N. Li, X. Lu, M. He, X. Duan and S. Wang, *J. Hazard. Mater.*, 2021, **414**, 125478.
17 T. Wang, W. M. de Vos and J. de Grooth, *J. Membr. Sci.*, 2022, **646**, 120209.
18 Y. Liu, Z. Song, W. Wang, Z. Wang, Y. Zhang, C. Liu, Y. Wang, A. Li, B. Xu and F. Qi, *Sep. Purif. Technol.*, 2021, **265**, 118268.
19 Y. Bao, T. T. Lim, R. Wang, R. Webster and X. Hu, *Chem. Eng. J.*, 2018, **343**, 737–747.
20 H. Jiang, S. Wang, Q. Chen, Y. Du and R. Chen, *Ind. Eng. Chem. Res.*, 2022, **61**, 7862–7873.
21 Z. Wang, Z. Chen, J. Chang, J. Shen, J. Kang and Q. Chen, *Chem. Eng. J.*, 2015, **262**, 904–912.
22 H. Park and H. Choi, *Water Res.*, 2011, **45**, 1933–1940.
23 B. Zhu, Y. Hu, S. Kennedy, N. Milne, G. Morris, W. Jin, S. Gray and M. Duke, *J. Membr. Sci.*, 2011, **378**, 61–72.
24 W. Lee, Y. Bao, X. Hu and T. T. Lim, *Chem. Eng. J.*, 2019, **378**, 121670.
25 S. Wang, J. Tian, Q. Wang, A. Zhao, F. Cui and G. Li, *J. Membr. Sci.*, 2019, **570**, 333–342.
26 Y. Guo, Z. Song, B. Hu, Y. Li, F. Qi, J. P. Croue and D. Yuan, *J. Hazard. Mater.*, 2018, **344**, 1229–1239.
27 Y. Guo, B. Xu and F. Qi, *Chem. Eng. J.*, 2016, **287**, 381–389.
28 S. Wang, J. Tian, Z. Wang, Q. Wang, J. Jia, X. Hao, S. Gao and F. Cui, *Chem. Eng. J.*, 2020, **396**, 125289.
29 C. Li, W. Sun, Z. Lu, X. Ao and S. Li, *Water Res.*, 2020, **175**, 115674.
30 B. Zhang, Y. Zhang, Y. Teng and M. Fan, *Crit. Rev. Environ. Sci. Technol.*, 2015, **45**, 1756–1800.

31 W. D. Oh, Z. Dong and T. T. Lim, *Appl. Catal., B*, 2016, **194**, 169–201.
32 S. Tian, Y. Liu, Y. Wang, J. Qi, L. Tian, J. Ma, G. Wen and L. Wang, *J. Hazard. Mater.*, 2022, **433**, 128819.
33 Z. Yang, D. Dai, Y. Yao, L. Chen, Q. Liu and L. Luo, *Chem. Eng. J.*, 2017, **322**, 546–555.
34 R. Yin, W. Guo, H. Wang, J. Du, X. Zhou, Q. Wu, H. Zheng, J. Chang and N. Ren, *Chem. Eng. J.*, 2018, **334**, 2539–2546.
35 Z. Xiao, Y. Li, L. Fan, Y. Wang and L. Li, *J. Colloid Interface Sci.*, 2021, **589**, 298–307.
36 K. Wang, D. Huang, W. Wang, Y. Li, L. Xu, J. Li, Y. Zhu and J. Niu, *Sci. Total Environ.*, 2021, **758**, 143666.
37 X. Du, W. Yang, Y. Liu, W. Zhang, Z. Wang, J. Nie, G. Li and H. Liang, *Sep. Purif. Technol.*, 2020, **252**, 117492.
38 I. Othman, Z. Zain, M. Abu Haija and F. Banat, *Appl. Catal., B*, 2020, **266**, 118601.
39 Y. Wang, Y. Zhang and J. Wang, *J. Membr. Sci.*, 2020, **615**, 118559.
40 M. C. Marti-Calatayud, E. Dionis, S. Mestre and V. Perez-Herranz, *J. Cleaner Prod.*, 2022, **363**, 132342.
41 Q. Zhao, D. Lu, H. Jiang, Y. Zhao, Y. Sun, Z. Li, M. Yang, P. Wang and J. Ma, *J. Membr. Sci.*, 2019, **573**, 210–217.
42 Q. Zhao, D. Lu, H. Jiang, Y. Zhao, Y. Sun, Z. Li, M. Yang, P. Wang and J. Ma, *J. Membr. Sci.*, 2019, **573**, 210–217.
43 X. Cheng, H. Liang, F. Qu, A. Ding, H. Chang, B. Liu, X. Tang, D. Wu and G. Li, *Chem. Eng. J.*, 2017, **308**, 1010–1020.
44 C. Wang, J. Zhao, C. Chen and P. Na, *Appl. Surf. Sci.*, 2021, **562**, 150134.
45 X. Li, Z. Ye, S. Xie, H. Li, Y. Lv, Y. Wang, Y. Wang and C. Lin, *J. Environ. Chem. Eng.*, 2022, **10**, 108264.
46 A. Rastogi, S. R. Ai-Abed and D. D. Dionysiou, *Appl. Catal., B*, 2009, **85**, 171–179.
47 Y. Guan, J. Ma, X. Li, J. Fang and L. Chen, *Environ. Sci. Technol.*, 2011, **45**, 9308–9314.
48 S. Liu, Z. Zhang, F. Huang, Y. Liu, L. Feng, J. Jiang, L. Zhang, F. Qi and C. Liu, *Appl. Catal., B*, 2021, **286**, 119921.
49 Q. Wang, H. Liu, P. Zhai, F. Sun, T. Chen, Z. Chu, D. Chen and X. Zou, *Chemosphere*, 2022, **305**, 135326.
50 Z. Wang, H. Qin and X. Liu, *Environ. Sci. Pollut. Res.*, 2019, **26**, 5904–5912.
51 S. Chen, X. Liu, S. Gao, Y. Chen, L. Rao, Y. Yao and Z. Wu, *Environ. Res.*, 2020, **183**, 109245.
52 L. Chen, T. Maqbool, W. Fu, Y. Yang, C. Hou, J. Guo and X. Zhang, *Sep. Purif. Technol.*, 2022, **295**, 121272.
53 W. Sang, Z. Li, M. Huang, X. Wu, D. Li, L. Mei and J. Cui, *Chem. Eng. J.*, 2020, **383**, 123057.
54 T. Zhang, Y. Chen, Y. Wang, J. Le Roux, Y. Yang and J.-P. Croué, *Environ. Sci. Technol.*, 2014, **48**, 5868–5875.